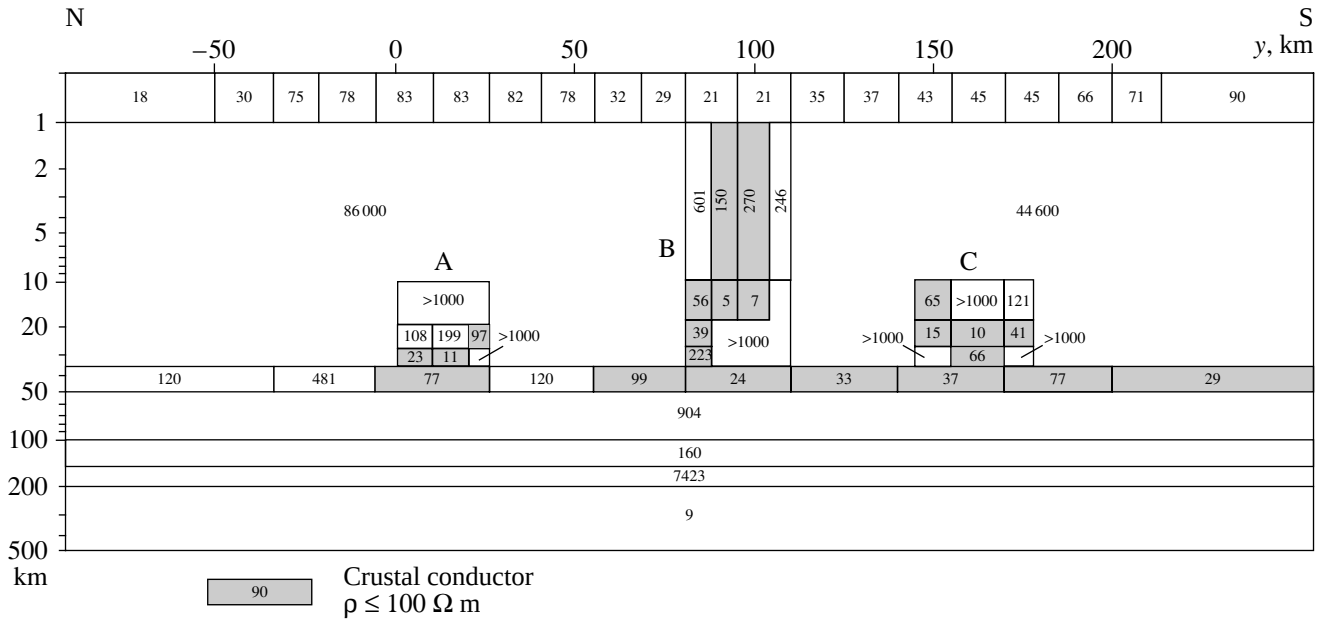

Fig. 15. The PI model: parallel inversion of $\mathrm{Re}\,W_{zy}$, $\mathrm{Im}\,W_{zy}$, $\varphi^{\parallel}$, $\rho^{\perp}$, and $\varphi^{\perp}$ using the II2DC program; resistivity values (in Ω m) are shown within blocks, and the region of lower crustal resistivities is shaded (cf. Fig. 4).

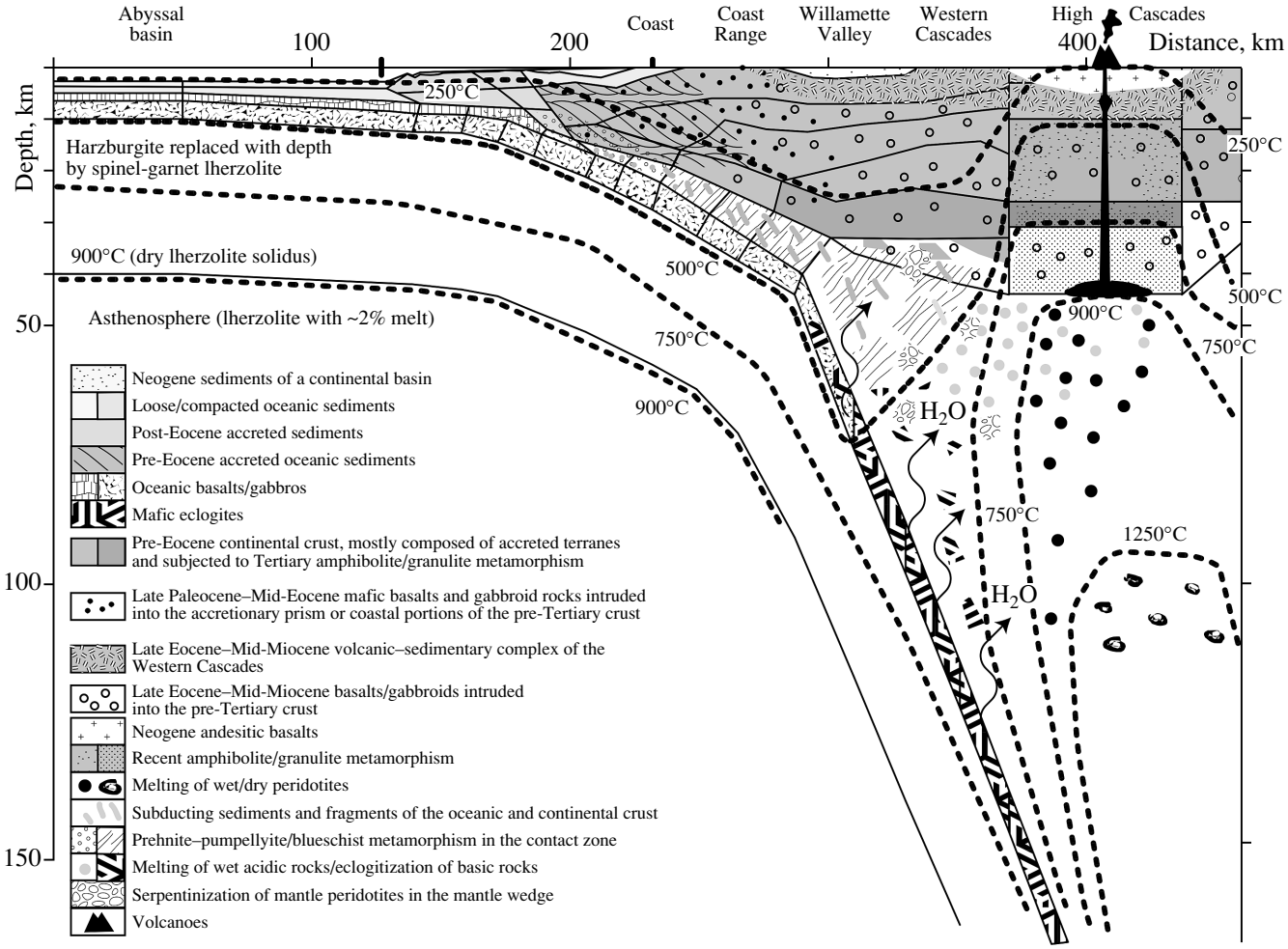

Fig. 16. Predictive geothermal and petrological CASCADIA model, constructed along an E–W profile across central Oregon [Romanyuk *et al.*, 2001].

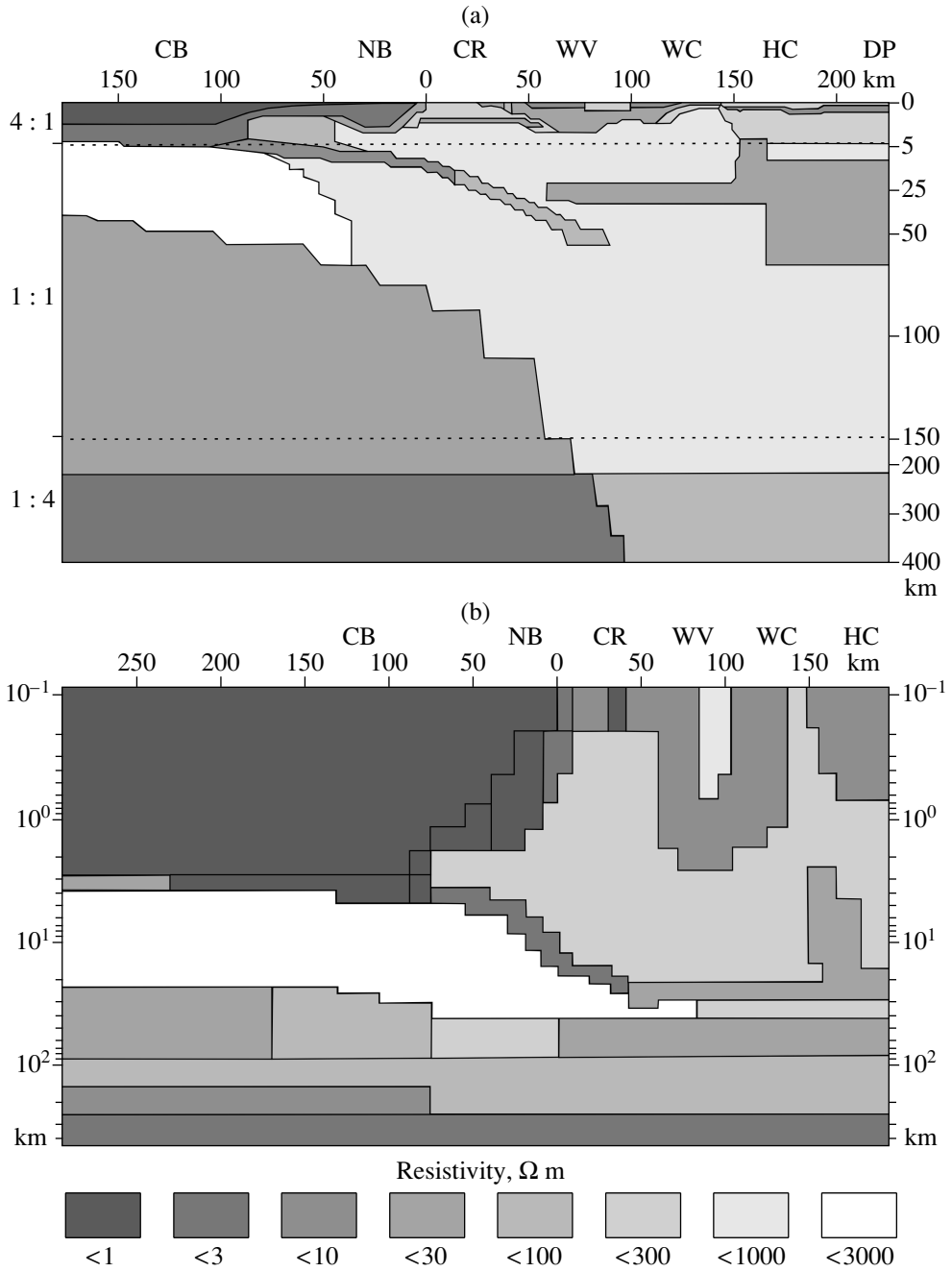

Fig. 17. Geoelectric models of the Cascadian subduction zone: (a) EMSLAB-I [Wannamaker *et al.*, 1989b]; (b) EMSLAB-II [Varentsov *et al.*, 1996]. CB, Cascadia basin; NB, Newport basin; CR, Coast Range; WV, Willamette Valley; WC, Western Cascades; HC, High Cascades; DP, Deschutes Plateau.

from the 2-D pattern. The EMSLAB-I model minimizes the misfits of the curves $\rho^{\perp}$ and $\varphi^{\perp}$ and ignores the curves $\rho^{\parallel}$ and $\varphi^{\parallel}$. Its main elements are (1) the upper conductive part of the plate, sinking at a low angle beneath the Coast Range; (2) a subhorizontal conducting layer in the middle continental crust broadening in the area of the High Cascades; and (3) a well-developed conductive asthenosphere beneath the ocean. The problem of the junction between the slab and the crustal conductor remains open in this model. The continental asthenosphere is not present in this model, although the shape of the experimental curves $\rho^{\parallel}$ and $\varphi^{\parallel}$ suggests a low resistivity of the upper mantle. The absence of large divergences between the model values of $\mathrm{Re}\, W_{zy}$ and $\mathrm{Im}\, W_{zy}$, on the one hand, and the experimental data, on the other hand, is considered by the authors as evidence of the reliability of the model.